# Multiple-excited-state absorption of $V^{2+}$ in low-field crystals: An *ab initio* model-potential embedded-cluster study

Sara López-Moraza, Luis Seijo, and Zoila Barandiarán*
*Departamento de Química, C-14, Universidad Autónoma de Madrid, 28049 Madrid, Spain*
(Received 1 October 1997)

In this paper we present an *ab initio* model-potential embedded-cluster study of the spin doublet excited states of $V^{2+}$-doped $KMgF_3$, $KZnF_3$, and $CsCaF_3$ fluoroperovskites, which includes intracluster electron correlation and quantum-mechanical lattice effects. The discrepancies of the calculated ground-state absorptions to the spin doublets with available experiments are systematic and amount to some 1000 $cm^{-1}$, leaving room for improvement of the treatment of valence electron correlation. The calculated excited-state absorption spectra originating in $^2E_g$ and $^2T_{1g}$ show that the broad $^2E_g, {}^2T_{1g} \rightarrow {}^2A_{1g}$ absorption bands considerably overlap the potential $^4T_{2g} \rightarrow {}^4A_{2g}$ laser emission, thus establishing a mechanism for laser loss that had not been considered so far in these low-field materials. The results obtained in these $V^{2+}$-doped fluoroperovskites, together with those in other $d^3$-doped low-field crystals, point out that the observed excited-state absorption spectra may correspond to either a single absorbing excited state or to the superposition of electronic transitions originating in all the different stable excited states lying below the energies used for pumping. Each of these excited states becomes a channel for absorptions that may result in multiple laser loss mechanisms. The separate study of each of these channels appears to be feasible using *ab initio* embedded-cluster methods. The conditions for the occurrence of single ($^4T_{2g}$) versus multiple ($^4T_{2g}, {}^2E_g, {}^2T_{1g}$) excited-state absorption, and, therefore, single versus multiple loss mechanisms, are discussed in this paper in terms of the energy barrier to $^2E_g, {}^2T_{1g} \rightarrow {}^4T_{2g}$ nonradiative decay. [S0163-1829(98)08019-9]

## I. INTRODUCTION

The knowledge of the excited-state absorption (ESA) spectra is considered to be one important clue to predict and understand the actual efficiency of potential solid-state laser materials. Excited-state absorptions from the laser level may overlap either pumping bands or the emission band, thus acting as a loss mechanism. The fact that some $V^{2+}$-doped fluoride crystals have been found to lase less efficiently than expected, led to experimental and theoretical investigations of the ESA properties of this $d^3$ defect in several hosts.[1–7] The possibility of a considerable overlap between the $^4T_{2g} \rightarrow {}^4A_{2g}$ emission band and the first $^4T_{2g} \rightarrow {}^4T_{1g}^a$ ESA band was expected: The experimental studies of the ESA spectra encountered considerable difficulties and showed low precision in the wavelength region of spontaneous emission;[5,6] their conclusions relative to the importance of this loss mechanism in $KMgF_3:V^{2+}$ (Refs. 5 and 6) were noncoincident. *Ab initio* model-potential (AIMP) embedded-cluster calculations of the $^4T_{2g} \rightarrow {}^4T_{1g}^a$ ESA electronic transition in this material showed no overlap with the emission band, in agreement with the observations of Moncorgé and Benyattou,[6] and the observed low laser efficiency is yet unexplained.

A recent theoretical investigation of the low-lying excited states of isoelectronic $Cr^{3+}$-doped low-field chloride and bromide elpasolites has shown a notable overlap between the spin-allowed $^2E_g \rightarrow {}^2A_{1g}$ ESA band and the emission band.[8] This fact suggests that the absorptions originating in the $^2E_g$ excited state could also be a channel for deactivation of the $V^{2+}$ lasers in low-field hosts and, therefore, it should be investigated.

Since the higher doublet excited states of $V^{2+}$ in low fields are difficult to see and assign in ground-state absorption spectra (they have low intensity and appear immersed in the broad spin-allowed absorption bands), it is not possible to infer the value of the $^2E_g \rightarrow {}^2A_{1g}$ nor the $^2T_{1g} \rightarrow {}^2A_{1g}$ absorption energies from the available experimental spectra. *Ab initio* embedded-cluster calculations represent an alternative to clarify whether these mechanisms are important or not in the lasing properties of new materials.

In this work, we have calculated the $^2E_g$ and $^2T_{1g}$ ESA electronic transitions of $V^{2+}$-doped $KMgF_3$, $KZnF_3$, and $CsCaF_3$. We have found that there is a very large overlap between the $^2E_g, {}^2T_{1g} \rightarrow {}^2A_{1g}$ ESA and the emission which should result in a notable loss of the laser efficiency.

## II. METHOD AND DETAILS OF THE CALCULATIONS

We have used the *ab initio* model-potential embedded-cluster method[9,10] (AIMP) to calculate the wave functions and energies of the local $^2E_g$, $^2T_{1g}$, $^2T_{2g}$, and $^2A_{1g}$ excited states of $V^{2+}$-doped $KMgF_3$, $KZnF_3$, and $CsCaF_3$ crystals. According to this method, the local electronic states of the imperfect $ABF_3:V^{2+}$ crystal, where the $V^{2+}$ impurities substitute for $Mg^{2+}$, $Zn^{2+}$, and $Ca^{2+}$ ions, respectively, in an octahedral site with coordination six, correspond to the wave functions and energies of the $(VF_6)^{4-}$ cluster embedded in the field of *ab initio* total ion model potentials, which represent the surrounding $A^+$, $B^{2+}$, $F^-$ ions.[9,10]

The $(VF_6)^{4-}$ embedded-cluster wave functions and energies were calculated using standard quantum-mechanical molecular programs.[11] The calculations presented here have been carried out using the same 176 contracted Gaussian

 © 1998 The American Physical Society

basis-set functions as in previous work on these materials.[7,12] The details of the embedding potentials used in this work to embed the $(VF_6)^{4-}$ cluster in the field of the $KMgF_3$, $KZnF_3$, and $CsCaF_3$ hosts are described in Ref. 12. In the study of the doublet excited states, we have used the embedding potentials referred to as AIMP/SM in Ref. 12, which also include lattice relaxation and dipole polarization.[13]

We performed the geometry optimization of the $^2E_g$, $^2T_{1g}$, $^2T_{2g}$, and $^2A_{1g}$ excited states of $ABF_3$:$(VF_6)^{4-}$ in the octahedral totally symmetric stretch coordinate in order to obtain impurity-ligand equilibrium distances and $a_{1g}$ vibrational frequencies. These geometry optimizations were performed with complete active space self-consistent field (CASSCF) calculations[14] including three active electrons in the five molecular orbitals that closely correspond to $V(3d)$. The calculations of the vertical electronic transitions corresponding to the ground-state absorptions to $^2E_g$, $^2T_{1g}$, $^2T_{2g}$, and $^2A_{1g}$ were done at the equilibrium geometry of the ground state $^4A_{2g}$ found in Ref. 12. The wave functions and energies were calculated using the aproximately size-consistent averaged coupled-pair functional (ACPF) method[15] where the previous CASSCF wave functions were used as the reference for dynamic correlation of 19 electrons. Single and double excitations were allowed from the mainly $3p(t_{1u})$ and $3d(t_{2g}$ and $e_g)$ vanadium orbitals and from a subset of the mainly $2p$ fluorine orbitals ($t_{2g}$ and $e_g$). This particular truncation of the valence electron correlation has been found to be a reasonable minimal treatment of the dynamical correlation, which brings the main corrections coming from the atomic metal correlation and the ligands correlation.[16] Since the $^4A_{2g}$ and the doublets ($^2E_g$, $^2T_{1g}$, $^2T_{2g}$, and $^2A_{1g}$) result from different terms of the free $V^{2+}$ ion, we calculated the error associated with truncation of the vanadium basis set and multiconfigurational expansion in the corresponding $^4F \rightarrow {}^2G$ free $V^{2+}$ ion using the same atomic basis set and correlation treatment as in the embeded-cluster systems. This error turned out to be $-1300$ cm$^{-1}$. We added this empirical correlation energy correction to the embeded-cluster ACPF electronic transitions.[17] The results of the calculated ground state absorptions and of the geometry optimizations are presented in Table I.

It can be seen that the equilibrium distances of the $^2E_g$ and $^2T_{1g}$ excited states in the three lattices differ by only 0.005, 0.005, and 0.002 Å, respectively, from that of the $^4A_{2g}$ ground state; in consequence, we calculated their excited-state absorptions as the corresponding vertical energy differences obtained at the ground-state equilibrium positions; they are presented in Table II.

## III. RESULTS AND DISCUSSION

The calculated ground-state electronic transitions can be compared with available experimental data in Table I. The results show a systematic error of about 1000 cm$^{-1}$, which should be associated to the limited treatment of ligand electron correlation. The neglect of spin-orbit and Jahn-Teller couplings in our calculations should not be responsible for the observed discrepancies: Only the $^4A_{2g} \rightarrow {}^2T_{1g}$ zero-phonon transition appears to be split by a very small spin-orbit coupling.[18] In order to facilitate the discussion of the results later on, we would like to compare the electronic transitions of Table I with previous calculations: All the spin doublets presented here are found to lie higher in energy than the first quartet excited state $^4T_{2g}$, the laser level ($^4A_{2g} \rightarrow {}^4T_{2g}$ was found to be: $KMgF_3$ 11 300, $KZnF_3$ 10 300, $CsCaF_3$ 9300 cm$^{-1}$ in Ref. 7); only the first two doublet excited states, $^2E_g$ and $^2T_{1g}$ are found to lie lower in energy than the second quartet excited state $^4T_{1g}^a$, the lowest level used for pumping ($^4A_{2g} \rightarrow {}^4T_{1g}^a$ was found to be $KMgF_3$ 18 200, $KZnF_3$ 16 900, $CsCaF_3$ 15 500 cm$^{-1}$ in Ref. 7), in agreement with the experiments.

In Table II we present the results of the calculated vertical excited-state absorption (ESA) energies. We have used as origins for ESA the two doublet excited states, which are found to be lower in energy than the first possible spin-allowed pumping band $^4A_{2g} \rightarrow {}^4T_{1g}^a$, namely, $^2E_g$ and $^2T_{1g}$. We have also inculded the results obtained previously for the $^4T_{2g} \rightarrow {}^4T_{1g}^a$ ESA,[7] using the same methodology plus $T \otimes e$ Jahn-Teller coupling of the $^4T_{2g}$ excited state, in order to show all the electronic transitions that we find in the infrared region of the ESA spectra.

In $KMgF_3$:$V^{2+}$, which is the only system where the ESA spectrum has been measured, our results show three sets of spin-allowed transitions: (i) $^2E_g, {}^2T_{1g} \rightarrow {}^2T_{2g}$ at 5900,5100 cm$^{-1}$, (ii) $^4T_{2g} \rightarrow {}^4T_{1g}^a$ at 6800,7300 cm$^{-1}$, which has been found to be slightly split by $T \otimes e$ Jahn-Teller coupling, and (iii) $^2E_g, {}^2T_{1g} \rightarrow {}^2A_{1g}$ at 9500,8700 cm$^{-1}$. The latter should be expected to be broad given the considerable difference in equilibrium geometries of the initial ($^2E_g, {}^2T_{1g}$) and final ($^2A_{1g}$) excited states, which amounts to some 0.03 Å (see Table I) and is comparable to that calculated for $^4A_{2g}$-$^4T_{2g}$ electronic states in these and similar systems. As we will discuss next, these results suggest a reinterpretation of one of the measured ESA spectra.[5]

Payne and co-workers measured the ESA spectra of $KMgF_3$:$V^{2+}$ at room temperature.[5] In the infrared region, it could not be scanned to frequencies greater than 8000 cm$^{-1}$ because the emission from the sample became too intense. Below this limit, they observed a rising broad feature (see Fig. 2 of Ref. 5). Although the authors comment that it is not clear how the infrared ESA curve should be extrapolated beyond the 8000 cm$^{-1}$ limit, they assigned the rising broad band observed to the $^4T_{2g} \rightarrow {}^4T_{1g}^a$ ESA and suggested that it should have its maximum intensity at frequencies greater than 8000 cm$^{-1}$ and full width at half-maximum (FWHM) greater than 2000 cm$^{-1}$, as indicated in Table II. Since, on the basis of the measured ground state absorption bands, the $^4T_{2g} \rightarrow {}^4T_{1g}^a$ ESA was expected to peak much lower in energy, at about 6400 cm$^{-1}$, and it was expected to be narrow, as it corresponds to an intraconfigurational transition,[19] Payne and co-workers justified their assignment by the reasonable suggestion of the existence of a strong $T \otimes e$ Jahn-Teller coupling in the $^4T_{2g}$ excited state with stabilization energy $E_{JT} > 400$ cm$^{-1}$ that would split the $^4T_{2g} \rightarrow {}^4T_{1g}^a$ into two bands: one at about 6800 cm$^{-1}$ (FWHM of about 1000 cm$^{-1}$), which the authors report as difficult to see in the noisy data, and another one at $>8000$ cm$^{-1}$ (FWHM $>$ 2000 cm$^{-1}$), which they associate to the rising broad band observed near the 8000 cm$^{-1}$ edge.[5] However, this interpretation, which was against the conclu-

TABLE I. Results of *ab initio* model potential embedded-cluster calculations in $V^{2+}$-doped fluoroperovskites.

| | $KMgF_3$ | $KZnF_3$ | $CsCaF_3$ |
|---|---|---|---|
| Ground-state absorption spectra ($cm^{-1}$): | | | |
| $^4A_{2g} \rightarrow {}^2E_g$ | | | |
| Calculated: | 13 525 | 13 503 | 13 464 |
| Experimental: | 12 670 [a] | | 12 597 [c] |
| $^4A_{2g} \rightarrow {}^2T_{1g}$ | | | |
| Calculated: | 14 323 | 14 311 | 14 273 |
| Experimental: | 13 340,13 375 [a] | | 12 952,12 958 [c] |
| $^4A_{2g} \rightarrow {}^2T_{2g}$ | | | |
| Calculated: | 19 452 | 19 203 | 18 906 |
| Experimental: | 18 430 [b] | | |
| $^4A_{2g} \rightarrow {}^2A_{1g}$ | | | |
| Calculated: | 23 040 | 22 018 | 20 976 |
| Calculated $a_{1g}$ equilibrium distances (Å) and vibrational frequencies ($cm^{-1}$): | | | |
| $^4A_{2g}$ [d] | 2.074, 545 | 2.105, 500 | 2.146, 450 |
| $^2E_g$ | 2.079, 543 | 2.110, 500 | 2.148, 451 |
| $^2T_{1g}$ | 2.079, 541 | 2.110, 499 | 2.148, 450 |
| $^2T_{2g}$ | 2.086, 542 | 2.118, 498 | 2.159, 447 |
| $^2A_{1g}$ | 2.103, 561 | 2.136, 516 | 2.177, 465 |

[a]Zero-phonon transition, Ref. 18.
[b]Phonon-assisted transition, Ref. 18.
[c]Zero-phonon transition, Ref. 3.
[d]Reference 12.

sions of previous experimental studies of the Jahn-Teller effects in $^4T_{2g}$ excited state,[18,20] is not supported by recent *ab initio* calculations of its $T \otimes e$ coupling,[7] which indicate that the Jahn-Teller effect is much weaker than suggested by Payne and co-workers.[5] This means that the rising broad feature observed in the infrared ESA spectra remains to be explained. In addition to this, the details of the ESA spectra between 5600 and 8000 $cm^{-1}$ (1800–1250 nm) shown in Fig. 2 of Ref. 5 and referred to as ''noisy data'' by the authors, would also require further explanation.

In effect, on the basis of the results of our calculations, shown in Table II, we propose the following interpretation of the observed ESA features.[5] (i) The broad rising band peaking at $> 8000$ $cm^{-1}$ with FWHM $> 2000$ $cm^{-1}$ should be assigned to the superposition of the $^2E_g, {}^2T_{1g} \rightarrow {}^2A_{1g}$ bands, both of which should be as broad as the ground-state spin-allowed absorption bands, given the comparable offshifts in equilibrium geometry of the connected electronic states. (ii) The lower-frequency region of the experimental ESA spectra shows a set of narrower peaks of lower intensity (Fig. 2 of Ref. 5), which fit quite well the remaining calculated electronic transitions. In fact, the peaks that can be read at about 5600,5800 $cm^{-1}$ (1800,1730 nm) compare very well with our $^2E_g, {}^2T_{1g} \rightarrow {}^2T_{2g}$ transitions. [The $^2E_g \rightarrow {}^2T_{2g}$ transition, which is shown to softly depend on the crystal field in Table II, is seen as a shoulder centered at 6500 $cm^{-1}$ in the higher-field $Gd_3Sc_2(GaO_4)_3:Cr^{3+}$ material[21] where it has been tentatively assigned to $^2E_g \rightarrow {}^2T_{2g}$.] Also, a series of increasingly intense unassigned shoulders/peaks read at about 6250, 6700, 7000, and 7400 $cm^{-1}$ (1600, 1500, 1425, and 1350 nm) fit well our calculated Jahn-Teller split $^4T_{2g} \rightarrow {}^4T_{1g}^a$ ESA. This assignment is also consistent with the band maximum observed at about 6800 $cm^{-1}$ in the infrared ESA scanned by Moncorgé and Benyattou up to 7250 $cm^{-1}$ in $KMgF_3:V^{2+}$ and displayed in Fig. 11 of Ref. 6.

Finally, if we compare the overall calculated infrared ESA with the emission bands (Table II), it is quite evident that the predominant loss mechanism for the laser emission in these crystals should not be the $^4T_{2g} \rightarrow {}^4T_{1g}^a$ transition, but, rather, the $^2E_g, {}^2T_{1g} \rightarrow {}^2A_{1g}$ broad absorption which should notably overlap the emission region.

TABLE II. Results of *ab initio* model potential embedded-cluster calculations of excited-state absorptions. Electronic transitions are not corrected by zero-point energy. All numbers in $cm^{-1}$.

| | $KMgF_3$ | $KZnF_3$ | $CsCaF_3$ | host effects ($CsCaF_3$–$KMgF_3$) |
|---|---|---|---|---|
| Calculated infrared excited state absorption spectra: | | | | |
| $^2T_{1g}\rightarrow{}^2T_{2g}$ | 5129 | 4892 | 4633 | –496 |
| $^2E_g\rightarrow{}^2T_{2g}$ | 5927 | 5700 | 5442 | –485 |
| $^4T_{2g}\rightarrow{}^4T_{1g}^a$ [a] | 6800,7300 | 6400,6900 | 6000,6400 | –800,–900 |
| $^2T_{1g}\rightarrow{}^2A_{1g}$ | 8717 | 7707 | 6703 | –2014 |
| $^2E_g\rightarrow{}^2A_{1g}$ | 9515 | 8515 | 7512 | –2003 |
| Experimental infrared excited state absorption spectra: | | | | |
| $^4T_{2g}\rightarrow{}^4T_{1g}^a$ [b] | peak $>8000$ FWHM $>2000$ | | | |
| $^4T_{2g}\rightarrow{}^4T_{1g}^a$ [c] | (6800) | | | |
| $^4T_{2g}\rightarrow{}^4A_{2g}$ emission: | | | | |
| Calculated [a] | 10000 | 9000 | 8100 | –1900 |
| Experimental [d] | 9070 | | 7400 | –1670 |

[a]Reference 7.
[b]Reference 5. FWHM stands for full width at half-maximum.
[c]From Fig. 11 of Ref. 6.
[d]Reference 4.

The reinterpretation that we propose of the measured infrared ESA spectra as being the result of multiple absorption from the $^4T_{2g}$ and the $^2E_g, {}^2T_{1g}$ excited states and, in consequence, the actual role of the ($^2E_g$, $^2T_{1g}$) ESA as a laser loss mechanism, rest upon the assumption that the doublets are also populated, to some extent, during the pumping of the sample. The stability of the doublet excited states is related to the energy separation between the ($^2E_g, {}^2T_{1g}$) and $^4T_{2g}$ excited states, which, ultimately, determine the population/depopulation of the doublets and, hence, the existence of multiple ($^4T_{2g}, {}^2E_g, {}^2T_{1g}$)/simple ($^4T_{2g}$) ESA. In this respect, it is interesting to analyze the barrier height for nonradiative $^2E_g\rightarrow{}^4T_{2g}$ (analogously, $^2T_{1g}\rightarrow{}^4T_{2g}$) decay: Our results show a notable barrier to nonradiative $^2E_g \rightarrow{}^4T_{2g}$ decay of some 1800 $cm^{-1}$ in the $V^{2+}$-doped crystal (see Fig. 1), which makes it reasonable to expect that the $^2E_g$ state is populated, to some significant extent, when the sample is excited. This should make it possible the occurrence of both $^2E_g$ emission and $^2E_g$ ESA. However, taking into account that spin-orbit coupling between $^2E_g$ and $^4T_{2g}$ should be very small (which is also related to the relatively large separation between $^2E_g$ and $^4T_{2g}$ at the minimum of $^2E_g$), the transition moment for $^2E_g\rightarrow{}^4A_{2g}$ emission should be very small and, therefore, the emission hardly seen, while for excitations from $^2E_g$ to the upper spin doublets, it should be comparable to that of the spin-allowed ground-state absorptions. All the same is true for the $^2T_{1g}$ excited state, whose energy separation and barrier height to nonradiative decay with respect to the laser level $^4T_{2g}$ can be also observed in Fig. 1. Therefore, in cases like $KMgF_3$:$V^{2+}$ (and $Cr^{3+}$-doped chlorides and bromides[8]) where the $^2E_g, {}^2T_{1g}-{}^4T_{2g}$ energy gap is relatively large, multiple excited-state absorption should be expected and the overlap between $^2E_g, {}^2T_{1g}\rightarrow{}^2A_{1g}$ ESA and $^4T_{2g}\rightarrow{}^4A_{2g}$ emission bands should become operative and notably detrimental of the laser efficiency.

One could expect that the overlap we have just discussed between ($^2E_g, {}^2T_{1g}$) ESA and emission could be a general loss mechanism for all $d^3$ impurities in low-field materials, since, according to the ligand field theory the energy differences ($^2E_g, {}^2T_{1g}$)$-{}^2A_{1g}$ and $^4A_{2g}-{}^4T_{2g}$ result from the crystal-field splitting of the atomic $^2G$ and $^4F$ terms, respectively. However, the occurrence of either single($^4T_{2g}$) or multiple ($^4T_{2g}, {}^2E_g, {}^2T_{1g}$) ESA, and, therefore, single or multiple loss mechanisms depend on the height of the energy barrier to ($^2E_g, {}^2T_{1g}$)$\rightarrow{}^4T_{2g}$ nonradiative decay, which is related to the nature of the transition-metal ion. In effect, it is interesting to observe the contrast between the barrier height to nonradiative decay found in $V^{2+}$-doped $KMgF_3$ (Fig. 1) with that calculated for the $Cr^{3+}$-doped $KMgF_3$ (Fig. 2), which are isoelectronic impurities in a common host. A negligible population of $^2E_g, {}^2T_{1g}$ should be expected in the case of $KMgF_3$:$Cr^{3+}$ due to the much smaller energy barrier to nonradiative decay to $^4T_{2g}$. This should result in that neither $^2E_g, {}^2T_{1g}\rightarrow{}^4A_{2g}$ emission nor ($^2E_g, {}^2T_{1g}$) ESA should significantly occur. Instead, simple $^4T_{2g}$ fluorescence and ESA spectra should be detected, the latter being the only possible ESA loss mechanism.

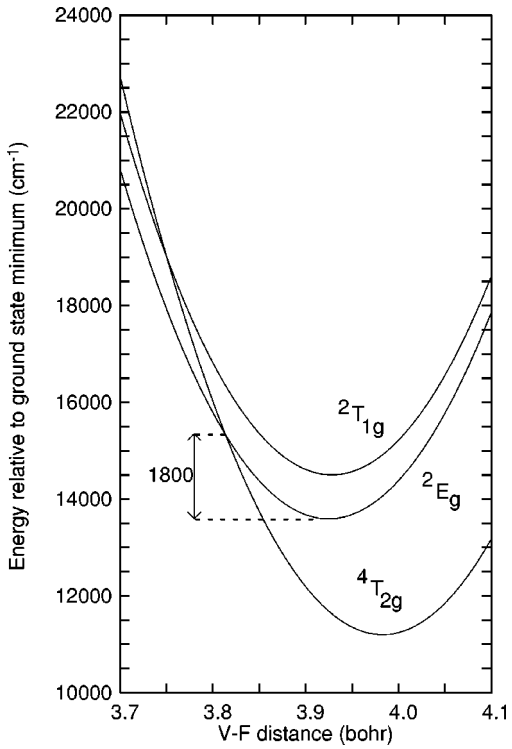


FIG. 1. Calculated potential energy surfaces of $^4T_{2g}$, $^2E_g$, and $^2T_{1g}$ excited states of $KMgF_3:V^{2+}$ along the totally symmetric stretching mode. The curvatures correspond to the CASSCF geometry optimizations. The curves are shifted along the energy scale so that the energy minima correspond to calculations performed at the ACPF level of methodology. The energy barrier to nonradiative decay down to the $^4T_{2g}$ is indicated in the figure for $^2E_g$ only. (1 bohr=0.529 177 Å).

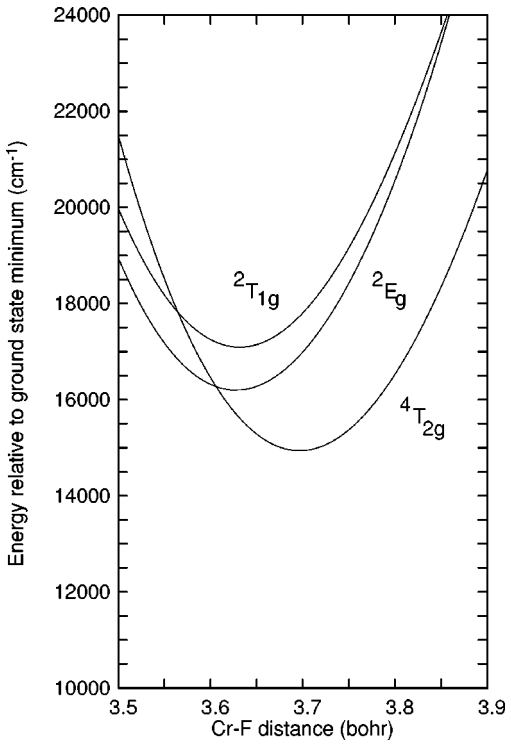


FIG. 2. Calculated potential energy surfaces of $^4T_{2g}$, $^2E_g$, and $^2T_{1g}$ excited states of $KMgF_3:Cr^{3+}$ along the totally symmetric stretching mode. The curvatures correspond to the CASSCF geometry optimizations. The curves are shifted along the energy scale so that the energy minima correspond to calculations performed at the ACPF level of methodology. (1 bohr=0.529 177 Å.)

Finally, we should mention the cases where $^2E_g$ and $^4T_{2g}$ are nearly degenerate, as in $Gd_3Sc_2(GaO_4)_3:Cr^{3+}$ material.[21] In these cases, multiple emission and ESA occur with dominance of the transitions originating in the $^4T_{2g}$ state.[21] The $^2E_g \rightarrow {}^4A_{2g}$ emission borrows its intensity from spin-orbit coupling with the almost degenerate $^4T_{2g}$; multiple ESA is observed as the superposition of all excited state absorptions leading to considerably structured ESA bands.[21]

## IV. CONCLUSIONS

The potential-energy surfaces of $^2E_g$, $^2T_{1g}$, $^2T_{2g}$, and $^2A_{1g}$ local electronic states, the ground-state absorptions $^4A_{2g} \rightarrow {}^2E_g, {}^2T_{1g}, {}^2T_{2g}, {}^2A_{1g}$, and the excited-state absorptions $^2E_g, {}^2T_{1g} \rightarrow {}^2T_{2g}, {}^2A_{1g}$ of $V^{2+}$-doped $KMgF_3$, $KZnF_3$, and $CsCaF_3$ fluoroperovskites, were calculated using the *ab initio* model-potential embedded-cluster method, which accounts for intracluster valence electron correlation and quantum-mechanical host effects. Our results showed that (a) the infrared excited-state absorption spectra are due to multiple absorptions from $^4T_{2g}$, $^2E_g$, and $^2T_{1g}$ excited states; this resulted in new assignments of part of the spectra that have been experimentally observed (b) the $^2E_g, {}^2T_{1g} \rightarrow {}^2A_{1g}$ transitions are expected to be as broad as the spin-allowed ground-state absorption bands and to overlap notably the $^4T_{2g} \rightarrow {}^4A_{2g}$ emission; this could be an explanation for the poorer than expected behavior of these systems as vibronic solid-state lasers. The occurrence of multiple ($^4T_{2g}$, $^2E_g$, $^2T_{1g}$) excited-state absorption in $V^{2+}$-doped fluoroperovskites was pointed out to be related to the existence of high-energy barriers to nonradiative $^2E_g, {}^2T_{1g} \rightarrow {}^4T_{2g}$ decay, which favors the population of the spin doublet excited states upon excitation of the sample. Conversely, single ($^4T_{2g}$) excited-state absorption was found to be related to fast nonradiative decays favored by small energy barriers, as was shown to be the case of $KMgF_3:Cr^{3+}$. The potentiality of materials showing multiple excited-state absorptions as vibronic solid state lasers should be considerably smaller.

## ACKNOWLEDGMENTS

This work was partly supported by a grant from MEC (DGICYT PB95-0201) Spain.

*Author to whom correspondence should be addressed. Electronic address: yara@sara.qfa.uam.es

[1] *Tunable Solid-State Lasers*, Vol. 47 of *Springer Series in Optical Science*, edited by P. Hammerling, A. B. Budgor, and A. Pinto (Springer, Berlin, 1985).

[2] *Tunable Solid-State Lasers II*, Vol. 52 of *Springer Series in Optical Science*, edited by A. B. Budgor, L. Esterowitz, and L. G. DeShazer (Springer, Berlin, 1986).

[3] U. Brauch and U. Dürr, Opt. Commun. **55**, 35 (1985).

[4] W. Knierim, A. Honold, U. Brauch, and U. Dürr, J. Opt. Soc. Am. B **3**, 119 (1986).

[5] S. A. Payne and L. L. Chase, J. Lumin. **38**, 187 (1987); S. A.

Payne, L. L. Chase, and G. D. Wilke, Phys. Rev. B **37**, 998 (1988).
[6] R. Moncorgé and T. Benyattou, Phys. Rev. B **37**, 9186 (1988).
[7] S. López-Moraza and Z. Barandiarán, J. Chem. Phys. **105**, 50 (1996).
[8] A. Al-Abdalla, Z. Barandiarán, and L. Seijo, J. Chem. Phys. **108**, 2005 (1998).
[9] Z. Barandiarán and L. Seijo, J. Chem. Phys. **89**, 5739 (1988).
[10] Z. Barandiarán and L. Seijo, in *Computational Chemistry: Structure, Interactions and Reactivity*, Vol. 77B of *Studies in Physical and Theoretical Chemistry*, edited by S. Fraga (Elsevier, Amsterdam, 1992), pp. 435–461.
[11] MOLCAS version 3, K. Andersson, M. R. A. Blomberg, M. P. Fülscher, V. Kellö, R. Lindh, P.-Å. Malmqvist, J. Noga, J. Olsen, B. O. Roos, A. J. Sadlej, P. E. M. Siegbahn, M. Urban, and P.-O. Widmark (University of Lund, Sweden, 1994).
[12] S. López-Moraza, J. L. Pascual, and Z. Barandiarán, J. Chem. Phys. **103**, 2117 (1995).
[13] J. L. Pascual and L. Seijo, J. Chem. Phys. **102**, 5368 (1995).
[14] B. O. Roos, P. R. Taylor, and P. E. M. Siegbahn, Chem. Phys. **48**, 157 (1980); P. E. M. Siegbahn, A. Heiberg, J. Almlöf, and B. O. Roos, J. Chem. Phys. **74**, 2384 (1981); P. Siegbahn, A. Heiberg, B. Roos, and B. Levy, Phys. Scr. **21**, 323 (1980).
[15] R. Ahlrichs, P. Scharf, and C. Ehrhardt, J. Chem. Phys. **82**, 890 (1985); R. J. Gdanitz and R. Ahlrichs, Chem. Phys. Lett. **143**, 413 (1988).
[16] K. Pierloot and L. G. Vanquickenborne, J. Chem. Phys. **93**, 4154 (1990).
[17] L. Pueyo and J. W. Richardson, J. Chem. Phys. **67**, 3583 (1977).
[18] M. D. Sturge, F. R. Merrit, L. F. Johnson, H. J. Guggenheim, and J. P. van der Ziel, J. Chem. Phys. **54**, 405 (1971).
[19] S. Sugano, Y. Tanabe, and H. Kamimura, *Multiplets of Transition-Metal Ions in Crystal* (Academic, New York, 1970).
[20] M. D. Sturge, Phys. Rev. B **1**, 1005 (1970).
[21] L. J. Andrews, S. M. Hitelman, M. Kokta, and D. Gabbe, J. Chem. Phys. **84**, 5229 (1986).
[22] *Ab initio* model potential embedded-cluster calculations in $KMgF_3:Cr^{3+}$ are in progress in our laboratory using the same methodology as in this paper.